Silencing microRNA-134 produces neuroprotective and prolonged seizure-suppressive effects

Eva M. Jimenez-Mateos , **Tobias Engel** , **Paula Merino-Serrais** , **Ross C. McKiernan** , **Katsuhiro Tanaka** , **Genshin Mouri** , **Takanori Sano** , **Colm O'Tuathaigh** , **John L. Waddington** , **Suzanne Prenter** , **Norman Delanty** , **Michael A. Farrell** , **Donncha F. O'Brien** , **Ronán M. Conroy** , **Raymond L. Stallings** , **Javier deFelipe** , and **David C. Henshall**

Abstract

Temporal lobe epilepsy is a common, chronic neurologic disorder characterized by recurrent spontaneous seizures. MicroRNAs (miRNAs) are small, non-coding RNAs that regulate post-transcriptional expression of protein-coding mRNAs, which may have important roles in the pathogenesis of neurologic disorders. In models of prolonged, injurious seizures (*status epilepticus*) and in experimental and human epilepsy, we found up-regulation of miR-134, a brain-specific, activity-regulated miRNA implicated in the control of dendritic spine morphology. Silencing of miR-134 expression *in vivo* using antagomirs reduced hippocampal CA3 pyramidal neuron dendrite spine density by 21%, and rendered mice refractory to seizures and hippocampal injury caused by *status epilepticus*. Depletion of miR-134 after *status epilepticus* reduced the later occurrence of spontaneous seizures by over 90% and mitigated attendant pathologic features of temporal lobe epilepsy. Thus, silencing miR-134 exerts prolonged seizure suppressant and neuroprotective actions; whether these represent anticonvulsant or truly antiepileptogenic effects requires additional experimentation.

Keywords

Dicer; Epileptogenesis; Hippocampal sclerosis; Synaptogenesis; Temporal lobe epilepsy

Epilepsy is a serious, chronic neurologic disorder characterized by recurrent spontaneous seizures which affects about 50 million people worldwide. Anti-epileptic drugs typically control seizures in two-thirds of patients but probably do not alter the underlying pathophysiology[1]. The development of symptomatic (acquired) epilepsy is thought to involve altered expression of ion channels, synaptic remodeling, inflammation, gliosis and neuronal death, among others[2–5]. However, few anti-epileptogenic interventions targeting these processes have shown sufficient efficacy *in vivo*[1], and our understanding of the cell and molecular mechanisms remains incomplete.

Evidence is emerging that microRNAs (miRNAs) may be critical to the pathogenesis of several neurologic disorders[6–7], including epilepsy[8–9]. MiRNAs are a family of small (~22 nt), endogenously expressed non-coding RNAs that regulate mRNA translation by imperfect base-pairing interactions within the 3′ untranslated region[10–11]. Depending on the degree of sequence complementarity, miRNA binding, which occurs via Argonaute proteins within the RNA-induced silencing complex (RISC), results in either cleavage or a reduction in the translational efficiency of the target mRNA[10–11].

MiR-134 is a brain-specific, activity-regulated miRNA implicated in the control of neuronal microstructure[12–13]. Pyramidal cells are the most common neurons in the neocortex and hippocampal formation[2]. They are the major source of intrinsic excitatory cortical synapses, and their dendritic spines are the main postsynaptic target of excitatory synapses, with spine size an index of synaptic strength[14–16]. Spine remodeling occurs during learning and memory formation, and in the setting of neuropsychiatric disorders and pathological brain activity[17–21]. Spine collapse is mediated in part by *N*-methyl-D-asparate (NMDA) receptor and calcium-dependent de-polymerization of actin by cofilin[19,22–23]. LIM kinase-1 (Limk1) phosphorylates and inactivates cofilin and loss of Limk1 results in abnormal spine morphology[24]. In hippocampal neurons, miR-134 targets *Limk1* mRNA, thereby preventing Limk1 protein translation[13]. Over-expression of miR-134 *in vitro* has been reported to reduce spine volume[13], whereas over-expression of miR-134 *in vivo* reduces total dendritic length[25] and abrogates long-term potentiation[26]. Mice lacking the miRNA biogenesis component DiGeorge syndrome critical region gene 8 fail to produce several mature miRNAs, including miR-134, and display reduced hippocampal spine density[27]. Spine loss may have divergent consequences according to context[28], promoting excitability[29] or uncoupling NMDA receptor-driven currents in neurons and preventing excitotoxicity[30].

Here we investigated the role of miR-134 in epilepsy and explored the *in vivo* effect of inhibiting miR-134. We report that miR-134 is up-regulated in experimental and human epilepsy and show that silencing miR-134 generates a seizure-refractory state and attenuates epileptic seizures and pathophysiological features of temporal lobe epilepsy (TLE).

Results

MiR-134 is regulated by *status epilepticus* and in epilepsy

We first investigated whether pathologic brain activity *in vivo* affects miR-134 levels. Prolonged seizures (*status epilepticus*, SE) were triggered by intra-amygdala microinjection of the glutamate receptor agonist kainic acid (KA) in mice[31–32]. The resultant seizures caused neuronal damage mainly within the hippocampal CA3 subfield (Fig. 1a) and triggered the later emergence of recurrent spontaneous (i.e. epileptic) seizures (Fig. 1f)[31].

To identify the cell populations expressing miR-134 *in vivo* we used *in situ* hybridization. Tissue sections labeled with a probe specific for mature miR-134 detected a strong signal in

the soma of hippocampal pyramidal neurons and hilar interneurons, as well as neurons in the neocortex and amygdala (Fig. 1b and Supplementary Fig. 1).

Real-time quantitative PCR (RT-qPCR) analysis showed SE resulted in an increase in mature miR-134 levels in the ipsilateral CA3 and CA1 subfields (Fig. 1c). Mature miR-134 levels were not changed in the undamaged contralateral CA3 (Supplementary Fig. 2a). Non-harmful, non-convulsive seizures, a model of epileptic preconditioning[33] in which SE does not develop, did not alter miR-134 levels compared to control in CA3 ($P = 0.89$) or CA1 ($P = 0.56$) ($n = 6$ per group, data not shown).

To determine whether miR-134 was functional, we measured levels within the RISC, where targeting of miRNAs to mRNA occurs[34]. Argonaute-2 was eluted from CA3[35–36] and miRNA extracted. A low level of miR-134 was detected in the RISC in controls, whereas levels of Argonaute-2-bound miR-134 were higher after SE (Fig. 1d). Protein levels of the miR-134 target, Limk1[13], were significantly lower in mice after SE (Fig. 1e).

We next investigated whether miR-134 and Limk1 expression was altered in experimental epilepsy. Spontaneous seizures emerge 3–4 days after SE in the present model[31,33] and within weeks animals display pathologic hallmarks of TLE, including neuron loss and astrogliosis (Fig. 1f). miR-134 levels were elevated one and three weeks after SE in CA1 and after three weeks in the CA3 of epileptic mice (Fig. 1g). Limk1 protein levels followed an opposite trend, being decreased in epileptic animals (Fig. 1h). Levels of Creb1, another validated miR-134 target[26], were also lower in epileptic mice (Supplementary Fig. 2b).

We next undertook an analysis of temporal lobe material from individuals with pharmacoresistent TLE. Higher levels of mature miR-134 were detected in TLE specimens compared to autopsy controls (Fig. 1i). This difference was not an artifact of post-mortem delay (Supplementary Fig. 2c–e). Protein levels of LIMK1 were lower in individuals with TLE compared to autopsy controls (Fig. 1i).

In vivo depletion of miR-134 using antagomirs

To explore the function of miR-134 *in vivo*, we injected mice with locked nucleic acid 3′ cholesterol-conjugated oligonucleotides ("antagomirs")[36–39]. Antagomirs targeting miR-134 (Ant-134) (Supplementary Fig. 3a) or a non-targeting scrambled sequence (Scr) were injected into the mouse ventricle (i.c.v.) (Supplementary Fig. 3b) and miRNA levels measured 1, 4, 8 or 12 h later, and after 1, 3, 5, 7 days, 1 and 2 months. A significant knockdown of miR-134 was first evident 12 h after injection of 0.12 nmol Ant-134 (Supplementary Fig. 4a–d), and by 24 h hippocampal levels of miR-134 were reduced by over 95% (Fig. 2a). This is similar to effects reported for antagomirs in other tissues[37]. Hippocampal levels of an unrelated miRNA, miR-19a, were not changed (Fig. 2b). Increasing the injected amount to 1 nmol appeared to produce off-target knockdown of miRNAs (Supplementary Fig. 4e,f). Levels of miR-134 began to recover by 7 days after Ant-134 injection although remained lower at 1 month, consistent with other reports[37], and had recovered by 2 months (Fig. 2c).

Brains from mice injected with antagomirs had grossly normal anatomy (data not shown). No evidence of hippocampal neuronal death was found when sections from mice injected with antagomirs were stained for Fluoro-Jade B (FJB), DNA fragmentation (terminal deoxynucleotidyl dUTP nick end labeling; TUNEL)[40], and the neuronal marker NeuN (Fig. 2d,e and data not shown).

To determine if reduction in the levels of miR-134 had any gross effects on animal behavior we performed ethological tests[41]. Mice were injected with either Scr or Ant-134 and

assessed 24 h later. No differences in ambulatory counts, distance travelled or vertical counts were found between groups (Fig. 2f), suggesting silencing of miR-134 does not alter normal exploratory activities.

miR-134 antagomirs reduce pyramidal neuron spine density

Because *in vitro* and *in vivo* evidence supports a role for miR-134 in controlling dendritic spine morphology[13,25,27], we examined whether antagomirs caused changes to dendritic spines *in vivo*. Individual CA3 pyramidal neurons in hippocampal slices from mice given 0.12 nmol Ant-134 or Scr 24 h earlier were microinjected with Lucifer Yellow and imaged using confocal microscopy, as described[42–43] (Fig. 3a, b).

Two-hundred eighteen neurons in Scr mice ($n = 7$) and 181 neurons in Ant-134 mice ($n = 7$) were analyzed. The structure of the basal dendritic tree was grossly normal between groups, as was the distribution of spines (Fig. 3c, e). Dendrites from Scr mice had an average of 68 nodes (ramifications) compared to 72 nodes in Ant-134 animals. The number of ramification points per μm was also similar (0.0127 nodes per μm in Scr compared to 0.0131 nodes per μm in Ant-134). We then analyzed spine density, assessing a total of 5343.7 μm length of dendrites in Scr mice (7455 spines) and a similar length (5477.5 μm) in Ant-134 animals (6196 spines). Spine density in Scr-injected animals was within the expected range[42] (Fig. 3d–f). Surprisingly, spine density was 21% lower in Ant-134 mice (Fig. 3d–f). Thus, injecting miR-134 antagomirs *in vivo* result in a significant reduction of spine density.

Silencing miR-134 inhibits SE and resultant neuronal death

To test the idea that antagomirs might influence pathologic brain activity *in vivo,* we compared seizures evoked by intra-amygdala KA between mice injected 24 h earlier with either Scr or Ant-134 (Fig. 4a and see Supplementary Fig. 3c). There was no difference in basal EEG between groups (Supplementary Fig. 5a). Scr-injected mice experienced typical SE, comprising episodes of high amplitude high frequency discharges (HAHFDs)[44] (compare Fig. 4c to Fig. 1a). EEG analysis revealed the duration of HAHFDs, which are associated with damage-causing pathologic activity[45], and total EEG power, were strongly reduced in Ant-134-injected mice (Fig. 4a–c). This effect was qualitatively similar to seizure suppression observed in animals given lorazepam 10 min before KA (compare Fig. 4c to Supplementary Fig. 5b).

miR-134 levels were reduced in mice injected with Ant-134 prior to intra-amygdala KA compared to Scr-treated animals (Fig. 4d and Supplementary Fig. 6a). Limk1 protein levels (Fig. 4e) and levels of Creb1 (Supplementary Fig. 6b) were lower after SE in Scr-injected mice, whereas levels of both were higher and similar to controls in animals injected with Ant-134 before KA.

We next examined hippocampal damage in tissue sections from Scr and Ant-134 mice. Scr-injected mice displayed typical CA3 lesions 24 h after SE, with extensive staining of neurons for FJB and TUNEL, and loss of NeuN staining (Fig. 5a–f). Mice injected with Ant-134 showed a dramatic reduction in each measure of seizure-induced neuronal death (Fig. 5a–f).

To specifically link the neuroprotective effects of antagomirs to miR-134 and Limk1, cultures of primary hippocampal neurons were treated with KA to model excitotoxic injury. Treatment with KA increased miR-134 levels (Fig. 5g). Ant-134 prevented KA-induced neurotoxicty in hippocampal neurons, and this was blocked in neurons transfected with short-hairpin RNAs targeting Limk1 (Fig. 5h–j).

Silencing miR-134 reduces spontaneous recurrent seizures

On the basis of findings so far, we hypothesized that silencing miR-134 might also affect epilepsy. To avoid a confounding influence of shortened SE duration or neuroprotection on epileptogenesis[40,46], we injected antagomirs 1 h after triggering SE. Analysis of EEG confirmed that when antagomirs were injected 1 h after KA, there was no difference in SE between Ant-134 and Scr groups (Fig. 6a). Also, CA3 damage assessed 24 h later was similar between Ant-134 and Scr animals (Fig. 6b,c).

We then equipped groups of mice with EEG telemetry units[31] and undertook continuous 24 h per day EEG recording for two weeks following SE. In agreement with the normal course of epilepsy in this model[31], mice injected with Scr after SE experienced the first spontaneous seizures on the third day, and all mice were epileptic by the fourth day (Fig. 6d,e and Supplementary Fig. 6c). The median epileptic seizure count for Scr-injected mice was 25 (range 8–79), with 200 epileptic seizures recorded in total (Fig. 6d and Supplementary Fig. 6c). In contrast, only 60% of mice injected with Ant-134 had had a spontaneous seizure by the 11th day after SE (Fig. 6d and Supplementary Fig. 6c); one mouse had only a single seizure on day 14, and another had no seizures (Fig. 6d). Ant-134-injected mice had a median epileptic seizure count of 2 (range 0–7), with just 16 epileptic seizures in total during the two week recording period ($P = 0.0001$, two-way ANOVA compared to Scr group) (Fig. 6e). The total amount of time spent in seizures also differed between groups ($P < 0.001$, two-way ANOVA, Supplementary Fig. 6c). The duration of individual epileptic seizures was similar between groups (Supplementary Fig. 6d).

Silencing miR-134 alters pathologic hallmarks of TLE

Progressive neuron loss, gliosis and rearrangement of mossy fibers are common pathological hallmarks of TLE[47–48]. Next, we examined whether Ant-134 had altered underlying pathology in the telemetry mice. Neuron counts in Ant-134-injected mice were higher than in Scr-treated animals at the end of epilepsy monitoring and astrogliosis was reduced (Fig. 6f). Neuropeptide Y (NPY) staining, an index of increasing reorganization of the hippocampus[33,49], in Scr-treated mice (Fig. 6g), was similar to previously reported scores in epileptic mice[33] whereas NPY scores in Ant-134 mice were significantly lower (Fig. 6g).

To investigate whether the reduced epileptic seizure rates were due to an anti-epileptogenic effect or a prolonged anticonvulsant effect of Ant-134, we performed additional experiments. First, we measured miR-134 levels in Ant-134 mice at the end of 14 days of telemetry recordings, which established levels were ~55% of those in Scr-injected animals (Supplementary Fig. 7a). Modeling this miR-134 reduction in mice did not produce an anticonvulsant effect against KA-induced SE (Supplementary Fig. 7b, c). Likewise, when Ant-134 was injected 14 days before KA this reduced levels of miR-134 to ~70% of Scr but mice were normally sensitive to KA-induced SE (Supplementary Fig. 7e–h), and animals were not protected against SE-induced damage (Supplementary Fig. 7i,j). Finally, longer-term video monitoring revealed mice given Ant-134 after SE displayed fewer generalized tonic-clonic seizures and more seizure-free days up to two months later compared to Scr-injected animals, although seizure rates did increase in 3 out of 5 animals (Fig. 6h,I and Supplementary Fig. 8).

Discussion

Our study shows silencing miR-134 in mice using antagomirs profoundly suppresses evoked seizures, the occurrence of spontaneous seizures and associated pathologic hallmarks of epilepsy. These are the first *in vivo* data to show that inhibition of a single mature miRNA

can alter pathologic electrical activity in brain and they offer a novel therapeutic target for the treatment of epilepsy.

An association between seizures and changes to miRNA expression has been suggested by recent profiling work[8–9,36,50], and by the phenotype of mice lacking Dicer[51], although our experiments are the first to link up-regulation of miR-134 to evoked, harmful seizures and chronic epilepsy. Brief, non-harmful generalized seizures were insufficient to alter miR-134 expression. This suggests *in vivo* regulation of miR-134 is not only a response to increased neuronal activity[13], but is coupled to epileptic or pathogenic brain activity. Critically, miRNA silencing experiments here support a role for miR-134 in facilitating pathologic neuronal activity *in vivo* because SE was potently suppressed in animals in which miR-134 was depleted by antagomirs. Notably, the seizure-suppressing effect of the antagomirs was nearly comparable to benzodiazepines[45–46,52]. Injecting antagomirs before SE also protected against seizure-damage. This probably arises because of shortened seizure duration[46,52] but antagomirs inhibited direct KA toxicity *in vitro*. Our *in vitro* experiments also implicated Limk1 in the mechanism of protection, but rescuing Creb1 levels may also contribute[53] and our data are consistent with the neuroprotective effect of sirtuin 1, which negatively regulates miR-134 expression in brain[26].

Despite progress in understanding the pathogenesis of epilepsy, few studies targeting epileptogenic processes have shown sufficient efficacy at reducing the occurrence, course or severity of the disease[1,54]. A second major finding here was that silencing miR-134 after SE resulted in a very substantial reduction of epileptic seizures in mice. Epilepsy developed normally in Scr-injected mice[31], whereas spontaneous seizures seldom occurred in Ant-134-treated animals. Thus, the effect was superior to neuroprotection applied at the time of SE[40,55] and comparable or exceeds the performance of other experimental anti-epileptogenic treatments[1]. Did the antagomirs interrupt epileptogenesis or simply prevent epileptic seizures from occurring due to a prolonged anticonvulsant effect or in a manner similar to anti-epileptic drugs? Spontaneous seizures were detected, albeit infrequently, and the increase in seizure rates over extended monitoring supports the interpretation of a prolonged anticonvulsant or anti-epileptic effect. Nevertheless, seizure rates never recovered to baseline and seizure frequency two months after SE, a time when antagomir suppression of miR-134 was no longer significant, was over 70% lower so an anti-epileptogenic effect remains possible. Additional experiments examining seizure frequency at time points later than two months will be required to distinguish these possibilities.

The mechanism by which miR-134 antagomirs suppressed seizures is unknown but our study offers the intriguing possibility that the effect is via changes to dendritic spines. The finding that Ant-134 reduced hippocampal CA3 dendritic spine density *in vivo* was surprising, and contrasts reports that spine size, not density, was controlled by miR-134[13]. Thus, a different phenotype results from miR-134 inhibition *in vivo,* which may be explained by the scale of miRNA suppression achieved, distribution of antagomir (somal versus dendritic), targets affected or potency of LNA-modified antagomirs over 2′-O-methyl-oligonucleotides[39]. Coincidently, a similar reduction in spine density was reported in mice lacking a miRNA biogenesis component, in which hippocampal levels of mature miR-134 were also reduced[27]. A key target of miR-134 is Limk1, which regulates dendritic spine dynamics[13]. Limk1 protein levels followed an opposite pattern to miR-134 expression and miR-134 silencing prevented seizure-induced down-regulation of Limk1, although other explanations for a decrease in spines are possible[15,56]. Could the reduction in spines account for seizure-suppression? Dendritic spines are targets of excitatory axons in the brain[14–15]. Although spines have been suggested to operate as barriers against potentially harmful afferent input[28], our data are consistent with evidence showing spine loss reduces excitatory responses[17,57], and transient spine reduction uncouples excitotoxic NMDA-mediated

signaling[30]. The antagomirs appear to curtail pathologic activity in brain without impairing tonic neuronal communication; this would have been detected by the ethogram, and is consistent with reports that a ~20% reduction in hippocampal pyramidal neuron spine numbers does not alter basal neurotransmission[58]. Spine-localized synaptic signaling is also implicated in the pathogenesis of TLE[3], but whether a similar mechanism may account for the seizure suppressant effects of miR-134 silencing is unknown. Loss of Limk1, which was countered via antagomirs, can result in increased hippocampal excitability[24]. However, other miR-134 targets with effects on excitability and seizure suppression are known[26,53].

While therapeutic application of miR-134 antagomirs for SE is probably barred by a need for pre-treatment, the longevity of the suppression after a single injection, consistent with antagomir data from mouse and primate experiments[37,39], suggests applications in refractory epilepsy or disease-modification in the wake of epilepsy-precipitating injuries. Alternate routes for antagomir deliver such as intra-nasal, as considered for anti-epileptic drug delivery[59], may avoid blood brain barrier exclusion of antagomirs *in vivo*[37], and facilitate translation to the clinic for the treatment of epilepsy.

ONLINE METHODS

Seizure models

All animal experiments were performed in accordance with the European Communities Council Directive (86/609/EEC) and were reviewed and approved by the Research Ethics Committee of the Royal College of Surgeons in Ireland (REC #205), under license from the Department of Health, Dublin, Ireland. Adult (20–22 g) male C57BL/6 mice (Harlan) were purchased from Harlan. Food and water was available *ad libitum*. Induction of SE was performed as described previously[31]. Mice were anesthetized with isoflurane and placed in a mouse-adapted stereotaxic frame. Following a midline scalp incision, Bregma was located and three partial craniectomies performed for placement of skull-mounted recording screws (Bilaney Consultants). A fourth craniectomy was drilled for placement of a guide cannula (Coordinates from Bregma; AP = −0.94 mm, L = −2.85 mm) based on a stereotaxic atlas[60]. The cannula and electrode assembly was fixed in place and the animal placed in an open Perspex box which allowed free movement. The EEG was recorded using a Grass Comet digital EEG. After baseline EEG was established, the animal was lightly restrained while an injection cannula was lowered 3.75 mm below the brain surface for injection of KA (Sigma-Aldrich) or vehicle (phosphate-buffered saline (PBS), pH adjusted to 7.4) into the basolateral amygdala nucleus. After 40 min, all mice received lorazepam (Ativan, 6 mg kg^{-1}, i.p.). Animals were recorded for up to an hour thereafter before being disconnected and placed in a warmed recovery chamber. Non-harmful seizures were induced by a single injection (i.p.) of KA (15 mg kg^{-1}), as described[36].

EEG analysis during SE

EEG was analyzed using TWinR software and the duration of HAHFDs, also termed as type IV seizures, was calculated between the time of KA injection and the time of lorazepam administration by an observer blinded to treatment group. Additional frequency and amplitude analysis of EEG was performed by uploading data to an automated programme for EEG analysis (LabChart Pro v7 software, ADInstruments Ltd).

Intracerebroventricular injections

For i.c.v. injections, additional mice were affixed with a cannula ipsilateral to the side of KA injection. Coordinates from Bregma were: AP = −0.3 mm, L = −1.0 mm, V = −2.0 mm. Mice received 1 μL infusion of either Scr or Ant-132 LNA- and 3′-cholesterol modified oligonucleotides (Exiqon) in aCSF (Harvard Apparatus). Mice were either euthanized or

underwent SE. For experiments involving intranasal administration of antagomirs, 0.12 nmol of scramble or antagomir in a 5 μl volume was administrated into each nostril of the mice. Mice were euthanized at various time points after antagomirs (1, 4, 8, 12 or 24 h, and 3, 5, 7, 14, 28 days and 2 months), after KA or vehicle (24 h), or once animals began to display spontaneous seizures at 1, 2, 4 or 8 weeks after intra-amygdala injections.

Analysis of spontaneous seizures using EEG telemetry

Epilepsy monitoring via implanted EEG telemetry units was performed as previously described[55]. EEG data were acquired with EEG transmitters (Model:F20-EET, Data Systems International) configured to record 2-channel EEG that were skull-affixed over dorsal hippocampi and temporal cortex under anaesthesia at the time of surgery for intra-amygdala injection. Transmitter units were placed in a subcutaneous pocket along the dorsal flank. Continuous (24 h per day) EEG data were collected for 14 consecutive days after SE. EEG data were reviewed and manually scored by an observer unaware of experimental treatment with epileptic seizures defined as high frequency (>5 Hz) high amplitude (>2 × baseline) polyspike discharges of ≥5 s duration.

Analysis of spontaneous seizures by continuous video monitoring

Mice were subjected to intra-amygdala KA-induced SE and then injected 1 h later with Scr or Ant-134 i.c.v., as before. Animals were allowed to recover and then housed in pairs (mice distinguished by ear clips) in clear Perspex cages (dimensions: 32 cm (long) × 17 cm (wide) × 14 cm deep). Webcam-style cameras connected to laptop computers were placed 40 cm from cages in a room equipped with safe lights for night-time recordings. Images were captured using VirtualDub 1.9.11 (SourceForge.net) with a sampling rate of 10 frames per second and data transfer rate of 140 kb s^{-1}. Videos from five days continuous (24 h per day) monitoring periods during weeks 3–4 and weeks 7–8 post-SE were reviewed by an observer unaware of experimental treatment. Seizures were counted using a modified 6-point Racine scale for mice. Score 2, Forelimb and or tail extension, rigid posture; 3, repetitive movements, head bobbing; Score 4, rearing and falling; Score 5, continuous rearing and falling; Score 6, severe tonic-clonic seizures. Note, clinical events below Score 2 (i.e. Score 1) such as sudden freezing and immobility were not included. The numbers of seizures per day was analyzed using Poisson regression with robust standard errors in order to express the experimental effect as an incidence rate ratio. Average Racine score and number of seizure-free days were compared using the Wilcoxon Mann-Whitney test.

Mouse tissue samples

Mice were killed by pentobarbital overdose and perfused with ice-cold saline to remove intravascular blood components. Brains for molecular and biochemical work were microdissected over wet ice with the hippocampus further sub-divided to obtain the separate CA3-enriched portion as described[55]. For histology, mice were either perfusion fixed with paraformaldehyde (4%) or brains fresh-frozen in 2-methylbutane (at −30 °C).

Human samples

This study was reviewed and approved by the Beaumont Hospital Ethics (Medical Research) Committee (approval REC 05/18) and informed consent was obtained from each subject. Subjects ($n = 3$) were determined to have medically intractable TLE and had been referred by an epileptologist (N.D.) for surgical resection of the temporal lobe (D. O'B) following neurological assessment, video-EEG recording and neuroimaging (magnetic resonance imaging). All patients were taking antiepileptic drugs prior to surgery. Each temporal lobe neocortex sample was inspected by a pathologist (M.F.) and deemed absent any obvious neuron loss or lesion. Subject 1 was a 27 year old male who underwent right posterior

temporal lobectomy. Subject 2 was a 53 year old male who underwent right anterior temporal lobectomy. Subject 3 was a 45 year old male who underwent temporal lobectomy. Temporal neocortex samples were flash-frozen in liquid nitrogen and stored at −70 °C until use. The sample was divided and used for either miRNA measurement or protein analysis.

Human control samples were also fresh-frozen and donated by people who died of causes not related to known neurological disease and obtained from the Brain and Tissue Bank for Developmental Disorders at the University of Maryland, Baltimore, Maryland, USA. Samples were all from people of caucasian race (Mean age 26.3 years, range 25 – 28). Causes of death were (for C1, C2) multiple injuries from road traffic accident, and (C3) cardiac tamponade. The average autopsy delay was 6.7 h (range 7–12 h).

Simulated post mortem delay

To simulate postmortem delay, mice were killed and cortices from the temporal association region extracted either immediately (0 h), or removed after a delay of 6 h or 12 h (simulated postmortem interval). Samples were then processed for miRNA measurement.

Histopathology

Coronal sections from two levels of dorsal (septal) hippocampus were analyzed (rostral, AP = −1.46 mm; medial, AP = −1.70 mm). For detection of neurodegeneration, sections were stained using FJB[55] (Millipore). Irreversible DNA damage was detected by Fluorescein-based TUNEL kit (Promega). For immunohistochemistry, sections were post-fixed, permeabilized, blocked in 5% goat serum and then incubated overnight with antibodies against NeuN (1:400, Clone A60, Millipore), GFAP (1:400, G9269) or NPY (1:1,000, N9528) (both from Sigma-Aldrich). Sections were washed and incubated with secondary antibodies raised in goat conjugated with AlexaFluor 488 (for NeuN) or AlexaFluor 568 (for GFAP and NPY) (BioSciences Ltd). Sections were mounted with medium containing 4′,6 diamidino-2-phenylindole (DAPI) (Vector Laboratories Ltd). Sections were examined using a Hamamatsu Orca 285 camera attached to a Nikon 2000s epifluorescence microscope (Micron-optical). Counts were the average of two adjacent sections of the ipsilateral CA3 subfield scored by an observer blinded to experimental treatment.

Synaptic reorganization was assessed blinded to experimental treatment in NPY-stained sections. Immunostaining was rated 0 to 5 using a scale adapted from methods of mossy fibre sprouting assessment[33]. Score 0, no NPY between the tips and crest of the dentate gyrus; Score 1, sparse staining in the supragranular region in a patchy distribution between the tips and crest of the dentate gyrus; Score 2, more abundant NPY in the supragranular region in a continuous distribution between tips and crest of the dentate gyrus; Score 3, prominent NPY in the supragranular region in a continuous pattern between tips and crest, with occasional patches of confluent staining between tips and crest of the dentate gyrus; Score 4, prominent NPY in the supragranular region that form a confluent dense laminar band between tips and crest; Score 5, confluent dense laminar band of NPY in the supragranular region that extends into the inner molecular layer.

miRNA expression

Total RNA was extracted using the miRNeasy kit (Qiagen) and 250 ng reverse transcribed using stem-loop Multiplex primer pools (Applied Biosystems). We used RT specific primers for mouse miRNAs miR-19a and miR-134 (Applied Biosystems) and qPCRs were carried out on a 7900HT Fast Realtime System (Applied Biosystems) using Taqman microRNA assays (Applied Biosystems). RNU19 or U6B was used for normalization. A relative fold change in expression of the target gene transcript was determined using the comparative cycle threshold method ($2^{-\Delta\Delta CT}$).

Western blotting

Protein was extracted from whole hippocampus or individual microdissected CA3 subfields, subjected to SDS-PAGE, transferred to nitrocellulose membranes and incubated with the following primary antibodies: Limk1 (1:1,000, Cat. 3842) and CREB (1:1,000, clone 86B10) (both from Cell Signaling Technology), β-Actin (1:2,000, clone AC40, Sigma-Aldrich), α-Tubulin (1:2,000, sc-8035) and GFP (1:500, sc-9996) (both from Santa Cruz Biotechnology). Membranes were then incubated with horseradish peroxidase-conjugated secondary antibodies (Jackson ImmunoResearch) and bands visualized using Supersignal West Pico Chemiluminescence Substrates (Pierce). Images were captured using a Fuji-Film LAS-300 and densitometry performed using AlphaEaseFC4.0 gel-scanning integrated optical density software (Alpha Innotech).

Argonaute-2 immunoprecipitation

Pools of three individual CA3 subfields for each condition were homogenized in immunoprecipitation buffer (300 mM NaCL, 5 mM $MgCl_2$, 0.1% NP-40, 50 mM Tris HCl pH7.5), centrifuged, and then 400 μl lysate incubated overnight at 4°C with 5 μg of antibodies against Argonaute-2 (C34C6, Cell Signaling Technology). Protein A-agarose beads (Santa Cruz Biotechnology) were added, mixed and incubated for 1 h at 4 °C, then centrifuged and the supernatant removed. The pellet was washed and processed for miRNA extraction, stem-loop reverse transcription and RT-PCR (Applied Biosystems).

In situ hybridization

Mice ($n = 3$) were perfused with 4% paraformaldehyde and 12 μm tissue sections mounted on SuperFrost-Plus slides (VWR). Using RNAse free solutions, slides were washed with RIPA buffer (150 mM NaCl, 1% IGEPAL, 0.5% Na deoxycholate, 0.1% SDS, 1 mM EDTA, 50 mM Tris pH 8.0) followed by treatment with 0.25% acetic anhydride in 0.1 M triethanolamine, rinsed with 0.1% Tween-20 in PBS and treated with 5 μg ml^{-1} Proteinase K. Next, slides were rinsed in hybridization buffer (1x saline solution, 50% formamide and 1X Denhardt's) for 1 h at 56 °C (melting temperature Tm-20C, Tm provided by Exiqon). The probe to detect miR-134 was the reverse complement to the mature miRNA and was 5′-digoxigenin-labeled,2′-O,4′-C methylene bicyclonucleoside monomer-containing oligonucleotide (LNA-modified). Probes were incubated 1:200 in hybridization buffer overnight at 56 °C in a humidified chamber. The following day sections were washed in FAM buffer (2x SSC, 50% formamide and 0.1% Tween 20) for 1 h at 60 °C. Then sections were rinsed in B1 buffer (150 mM NaCl, 100 mM Maleic acid and 0.4% IGEPAL pH:7.5) for 1 h at room temperature and B2 buffer (2% blocking reagent and 10% goat serum in B1) for 30 min. Polyclonal antibodies against digoxigenin (1:1000, Cat. 11093274910, Roche) were incubated in B2 overnight at 4 °C. The following day sections were washed in B1 buffer and incubated in B3 buffer (100 mM NaCl, 50 mM $MgCl_2$, 0.025% Tween 20 and 100 mM Trizma pH 9.5) for 30 min. Then 200 μl of color substrate solution (CSS: Nitroblue tetrazolium in BCIP stock solution (Roche) diluted 1:50 in B3 buffer) was added to each slide until the signal appeared. Slides were then rinsed, mounted with medium and coverslipped.

Antagomirs

Scr or Ant-134 (Exiqon, LNA- and 3′-cholesterol modified oligonucleotides) in artificial cerebrospinal fluid (aCSF) (Harvard Apparatus) was injected into the lateral ventricle of the mouse.

Behaviour analysis

Exploratory activity was assessed in Ant-134 and Scr-injected mice in the open field. Each mouse was placed individually in the centre of an open field apparatus (ENV-510; 27.9 × 27.9 cm; Med Associates). Total ambulatory counts, distance travelled (cm), and vertical counts were recorded. Data were collected over a 60 min period.

Spine density analysis

Coronal mouse brain sections (150 μm) were cut on a vibratome and pre-labeled with DAPI. Pyramidal cells from the CA3 subfield were individually injected with Lucifer yellow (8% in 0.1 M Tris buffer, pH 7.4). Lucifer Yellow was applied to each injected cell by continuous current until the individual dendrites of each cell could be traced to an abrupt end at their distal tips that fluoresced brightly. Sections were then processed with a rabbit polyclonal antibody against Lucifer Yellow produced at the Cajal Institute [1:400,000 in 2% bovine serum albumin (A3425; Sigma-Aldrich), 1% Triton X-100, 5% sucrose in phosphate buffer] followed by a streptavidin coupled to Alexafluor 488 (1:1000; Molecular Probes). The sections were washed and mounted with ProLong Gold Antifade Reagent (Invitrogen). For each pyramidal neuron (4–7 neurons from each mouse, 7 mice per group, 83 neurons total), 1 randomly selected dendrite was scanned from the soma to the tip. Images of dendrites from Scr and Ant-134 mice ($n = 40$) were acquired with a Zeiss (LSM 710) confocal laser scanning microscope and fluorescence of AlexaFluor 488 was recorded. Image stacks were obtained that consisted of 10–100 image planes (voxel size, 0.057 × 0.057 × 0.14 μm and area 58.36 × 58.36 μm) with a 63x oil-immersion lens (AN, 1.40; refraction index 1.45) using a calculated optimal zoom factor 2.3. For each stack, laser intensity and detector sensitivity were set so that the fluorescence signal from the dendritic spines occupied the full dynamic range of the detector. Therefore, some pixels were saturated in the dendritic shaft, but no pixels were saturated within the dendritic spines. After the acquisition, stacks were opened with Imaris 7.1 (Bitplane AG). The images were coded and not broken until the quantitative analysis had been completed. After acquisition, the stacks were processed with a three-dimensional blind deconvolution algorithm (Autodeblur; Autoquant, Media Cybernetics) for 10 iterations to reduce the out-of-focus light. Image stacks were imported to the confocal module of Neurolucida 8.03 (MicroBrightfield, Inc.) and dendritic spine density was determined by tracing the image of the acquired dendrites in three dimensions. Spines were marked during tracing and all protrusions were considered spines. After tracing the reconstructed data were exported to Neurolucida Explorer (MicroBrightField Inc.) for quantitative analysis. The spine density was calculated for each dendrite by dividing its length by the number of spines, and the spine density was also analyzed as a function of its distance from soma (Sholl analysis) by dividing the length of the dendritic segment by the number of spines in this distance for every 10 μm distance from the soma.

Cell culture

SH-SY5Y cells were grown in 10% fetal calf serum, 2 mM glutamine and 100 U ml^{-1} penicillin and streptomycin in Dubelco's Modified Eagle Medium/Ham's F12. Cells were maintained at 37 °C in a humidified atmosphere of 5% CO_2. Hippocampal neurons were prepared from gestational day 18 embryos (E18). The harvested embryos were transferred to Hank's balanced salt solution without calcium and magnesium medium (Invitrogen), hippocampi isolated, and the surrounding meninges were removed. The tissue was then incubated with Papain (Worthington Biochemical Corp.) for 30 min, the cells were gently dissociated, counted and then seeded in dishes coated with 1 mg ml^{-1} poly(L-lysine) and 20 μg ml^{-1} Laminin in Horse Serum/Neurobasal medium (10% Horse Serum, 2 mM Glutamine, 2 mM pyruvate and 100 U ml^{-1} penicillin/streptomycin in Neurobasal medium). After 3 h, the medium was removed and N2/B27/Neurobasal medium (N2 (Invitrogen), B27

(Invitrogen) 2 mM Glutamine, 2 mM pyruvate and 100 U ml^{-1} penicillin/streptomycin in Neurobasal medium) was added. Half of the N2/B27/Neurobasal medium was replaced every 2 days.

Two days after transfection, hippocampal neurons were exposed to 0.3 μM KA for 6 h and then neuronal damage was assessed. Neurons were live-stained with Hoechst 33258 (1 μg ml^{-1}) and propidium iodide (5 μM) in the medium for 30 min. Nuclear morphology was assessed with an epifluorescence microscope under 20x objective. For each condition, images of nuclei were captured in six different areas for each individual experiment. GFP and PI positive cells showing condensed and/or fragmented nuclei were scored as dead and expressed as a percentage of the total GFP positive cell population.

Plasmids and transfection

SH-SY5Y cells were transfected using lipofectamine 2000 (Invitrogen). Briefly, DNA was incubated with the lipofectamine reagent for 20 min in a ratio of 1:2 v/v. Then, the DNA:Lipofectamine mix was added to the cells for 4 h. Medium was removed, cells washed and new medium was added. Two days later, cells were harvested and samples prepare for western blotting. Hippocampal neurons were transfected at DIV6 with 3 μg of the expression plasmid pGFP-V-RS-scramble or pGFP-V-RS -shLimk (Origen) and 0.01 nmol of either Scr or Ant-134 (Exiqon) using calcium-phosphate technique. The following sequences were used:

sh-Control: GCACTACCAGAGCTAACTCAGATACTACT

shLimk1: AAGGACAAGAGGCTCAACTTCATCACTGA

sh-Limk2: CTGGCACGCAGACTGCTTCAGGTGTTGTG

Data analysis

All data are presented as the means ± standard error of the mean (s.e.m.). Two group comparisons were made using unpaired Student's t-test, while multi-group comparisons were made using one or two-way analysis of variance (ANOVA) followed by appropriate *post hoc* testing (GraphPad Instat). Significance was accepted at $P < 0.05$.

Supplementary Material

Refer to Web version on PubMed Central for supplementary material.

Acknowledgments

The authors would like to thank J. Varley, J. Phillips and members of the Epilepsy Programme, Beaumont Hospital. We thank S. Miller-Delaney for assistance and N. Plesnila, J. Prehn and R. Simon for helpful suggestions on the manuscript. We thank the Brain and Tissue Bank for Developmental Disorders at the University of Maryland, Baltimore, Maryland. This work was supported by funding from Science Foundation Ireland awards 08/IN1/B1875 (D.C.H., E.J-M., K.T., G.M., T.S.), 11/TIDA/B1988 (D.C.H.) and 07/IN.1/B960 (J.W., C.O'T.), US National Institute of Neurological Disorders and Stroke award R56 073714 (D.C.H.) an Irish Research Council for Science, Engineering and Technology postdoctoral fellowship (E. J-M.), Irish Health Research Board grant PHD/2007/11 (R.M.), and the Spanish Ministry of Education, Science and Innovation grant SAF2009-09394 (J.F.).

Pitkanen A, Lukasiuk K. Mechanisms of epileptogenesis and potential treatment targets. Lancet Neurol. 2011; 10:173–186. [PubMed: 21256455]

DeFelipe J. Chandelier cells and epilepsy. Brain. 1999; 122:1807–1822. [PubMed: 10506085]

McNamara JO, Huang YZ, Leonard AS. Molecular signaling mechanisms underlying epileptogenesis. Sci STKE. 2006; 2006:re12. [PubMed: 17033045]

Wetherington J, Serrano G, Dingledine R. Astrocytes in the epileptic brain. Neuron. 2008; 58:168–178. [PubMed: 18439402]

Vezzani A, French J, Bartfai T, Baram TZ. The role of inflammation in epilepsy. Nat Rev Neurol. 2011; 7:31–40. [PubMed: 21135885]

Eacker SM, Dawson TM, Dawson VL. Understanding microRNAs in neurodegeneration. Nat Rev Neurosci. 2009; 10:837–841. [PubMed: 19904280]

Saugstad JA. MicroRNAs as effectors of brain function with roles in ischemia and injury, neuroprotection, and neurodegeneration. J Cereb Blood Flow Metab. 2010; 30:1564–1576. [PubMed: 20606686]

Aronica E, et al. Expression pattern of miR-146a, an inflammation-associated microRNA, in experimental and human temporal lobe epilepsy. Eur J Neurosci. 2010; 31:1100–1107. [PubMed: 20214679]

Song YJ, et al. Temporal lobe epilepsy induces differential expression of hippocampal miRNAs including let-7e and miR-23a/b. Brain Res. 2011; 1387:134–140. [PubMed: 21376023]

Ambros V. The functions of animal microRNAs. Nature. 2004; 431:350–355. [PubMed: 15372042]

Bartel DP. MicroRNAs: genomics, biogenesis, mechanism, and function. Cell. 2004; 116:281–297. [PubMed: 14744438]

Lagos-Quintana M, et al. Identification of tissue-specific microRNAs from mouse. Curr Biol. 2002; 12:735–739. [PubMed: 12007417]

Schratt GM, et al. A brain-specific microRNA regulates dendritic spine development. Nature. 2006; 439:283–289. [PubMed: 16421561]

Matsuzaki M, Honkura N, Ellis-Davies GC, Kasai H. Structural basis of long-term potentiation in single dendritic spines. Nature. 2004; 429:761–766. [PubMed: 15190253]

Zhou Q, Homma KJ, Poo MM. Shrinkage of dendritic spines associated with long-term depression of hippocampal synapses. Neuron. 2004; 44:749–757. [PubMed: 15572107]

Noguchi J, Matsuzaki M, Ellis-Davies GC, Kasai H. Spine-neck geometry determines NMDA receptor-dependent Ca2+ signaling in dendrites. Neuron. 2005; 46:609–622. [PubMed: 15944129]

Muller M, Gahwiler BH, Rietschin L, Thompson SM. Reversible loss of dendritic spines and altered excitability after chronic epilepsy in hippocampal slice cultures. Proc Natl Acad Sci USA. 1993; 90:257–261. [PubMed: 8093558]

Rensing N, et al. In vivo imaging of dendritic spines during electrographic seizures. Ann Neurol. 2005; 58:888–898. [PubMed: 16240365]

Zeng LH, et al. Kainate seizures cause acute dendritic injury and actin depolymerization in vivo. J Neurosci. 2007; 27:11604–11613. [PubMed: 17959803]

Penzes P, Cahill ME, Jones KA, VanLeeuwen JE, Woolfrey KM. Dendritic spine pathology in neuropsychiatric disorders. Nat Neurosci. 2011; 14:285–293. [PubMed: 21346746]

Bhatt DH, Zhang S, Gan WB. Dendritic spine dynamics. Annu Rev Physiol. 2009; 71:261–282. [PubMed: 19575680]

Halpain S, Hipolito A, Saffer L. Regulation of F-actin stability in dendritic spines by glutamate receptors and calcineurin. J Neurosci. 1998; 18:9835–9844. [PubMed: 9822742]

Saneyoshi T, Fortin DA, Soderling TR. Regulation of spine and synapse formation by activity-dependent intracellular signaling pathways. Curr Opin Neurobiol. 2010; 20:108–115. [PubMed: 19896363]

Meng Y, et al. Abnormal spine morphology and enhanced LTP in LIMK-1 knockout mice. Neuron. 2002; 35:121–133. [PubMed: 12123613]

Christensen M, Larsen LA, Kauppinen S, Schratt G. Recombinant Adeno-Associated Virus-Mediated microRNA Delivery into the Postnatal Mouse Brain Reveals a Role for miR-134 in Dendritogenesis in Vivo. Front Neural Circuits. 2010; 3:16. [PubMed: 20126250]

Gao J, et al. A novel pathway regulates memory and plasticity via SIRT1 and miR-134. Nature. 2010; 466:1105–1109. [PubMed: 20622856]

Stark KL, et al. Altered brain microRNA biogenesis contributes to phenotypic deficits in a 22q11-deletion mouse model. Nat Genet. 2008; 40:751–760. [PubMed: 18469815]

Segal M. Dendritic spines, synaptic plasticity and neuronal survival: activity shapes dendritic spines to enhance neuronal viability. Eur J Neurosci. 2010; 31:2178–2184. [PubMed: 20550565]

Sierra-Paredes G, Oreiro-Garcia T, Nunez-Rodriguez A, Vazquez-Lopez A, Sierra-Marcuno G. Seizures induced by in vivo latrunculin a and jasplakinolide microperfusion in the rat hippocampus. J Mol Neurosci. 2006; 28:151–160. [PubMed: 16679555]

Meller R, et al. Ubiquitin proteasome-mediated synaptic reorganization: a novel mechanism underlying rapid ischemic tolerance. J Neurosci. 2008; 28:50–59. [PubMed: 18171922]

Mouri G, et al. Unilateral hippocampal CA3-predominant damage and short latency epileptogenesis after intra-amygdala microinjection of kainic acid in mice. Brain Res. 2008; 1213:140–151. [PubMed: 18455706]

Murphy BM, et al. Contrasting patterns of Bim induction and neuroprotection in Bim-deficient mice between hippocampus and neocortex after status epilepticus. Cell Death Differ. 2010; 17:459–468. [PubMed: 19779495]

Jimenez-Mateos EM, Mouri G, Conroy RM, Henshall DC. Epileptic tolerance is associated with enduring neuroprotection and uncoupling of the relationship between CA3 damage, neuropeptide Y rearrangement and spontaneous seizures following intra-amygdala kainic acid-induced status epilepticus in mice. Neuroscience. 2010; 171:556–565. [PubMed: 20837105]

Peters L, Meister G. Argonaute proteins: mediators of RNA silencing. Mol Cell. 2007; 26:611–623. [PubMed: 17560368]

Karginov FV, et al. A biochemical approach to identifying microRNA targets. Proc Natl Acad Sci USA. 2007; 104:19291–19296. [PubMed: 18042700]

Jimenez-Mateos EM, et al. MicroRNA expression profile after status epilepticus and hippocampal neuroprotection by targeting miR-132. Am J Pathol. 2011; 179:2519–2532. [PubMed: 21945804]

Krutzfeldt J, et al. Silencing of microRNAs in vivo with 'antagomirs'. Nature. 2005; 438:685–689. [PubMed: 16258535]

Krutzfeldt J, et al. Specificity, duplex degradation and subcellular localization of antagomirs. Nucleic Acids Res. 2007; 35:2885–2892. [PubMed: 17439965]

Elmen J, et al. LNA-mediated microRNA silencing in non-human primates. Nature. 2008; 452:896–899. [PubMed: 18368051]

Engel T, et al. Reduced hippocampal damage and epileptic seizures after status epilepticus in mice lacking proapoptotic Puma. FASEB J. 2010; 24:853–861. [PubMed: 19890018]

O'Tuathaigh CM, et al. Phenotypic characterization of spatial cognition and social behavior in mice with 'knockout' of the schizophrenia risk gene neuregulin 1. Neuroscience. 2007; 147:18–27. [PubMed: 17512671]

Merino-Serrais P, Knafo S, Alonso-Nanclares L, Fernaud-Espinosa I, Defelipe J. Layer-specific alterations to CA1 dendritic spines in a mouse model of Alzheimer's disease. Hippocampus. 2011; 21:1037–1044. [PubMed: 20848609]

Ballesteros-Yanez I, Benavides-Piccione R, Bourgeois JP, Changeux JP, DeFelipe J. Alterations of cortical pyramidal neurons in mice lacking high-affinity nicotinic receptors. Proc Natl Acad Sci USA. 2010; 107:11567–11572. [PubMed: 20534523]

Engel T, et al. Loss of p53 results in protracted electrographic seizures and development of an aggravated epileptic phenotype following status epilepticus. Cell Death Dis. 2010; 1:e79. [PubMed: 21368852]

Shinoda S, et al. Development of a model of seizure-induced hippocampal injury with features of programmed cell death in the BALB/c mouse. J Neurosci Res. 2004; 76:121–128. [PubMed: 15048936]

Pitkanen A, Kharatishvili I, Narkilahti S, Lukasiuk K, Nissinen J. Administration of diazepam during status epilepticus reduces development and severity of epilepsy in rat. Epilepsy Res. 2005; 63:27–42. [PubMed: 15716080]

Nairismagi J, et al. Progression of brain damage after status epilepticus and its association with epileptogenesis: a quantitative MRI study in a rat model of temporal lobe epilepsy. Epilepsia. 2004; 45:1024–1034. [PubMed: 15329065]

Mathern, GW.; Babb, TL.; Armstrong, DL. Hippocampal Sclerosis. In: Engel, JJ.; Pedley, TA., editors. Epilepsy: a comprehensive textbook. Vol. 13. Lippincott-Raven Publishers; Philadelphia: 1997. p. 133-155.

Cavazos JE, Golarai G, Sutula TP. Mossy fiber synaptic reorganization induced by kindling: time course of development, progression, and permanence. J Neurosci. 1991; 11:2795–2803. [PubMed: 1880549]

Hu K, et al. Expression profile of microRNAs in rat hippocampus following lithium-pilocarpine-induced status epilepticus. Neurosci Lett. 2011; 488:252–257. [PubMed: 21094214]

Tao J, et al. Deletion of astroglial dicer causes non-cell-autonomous neuronal dysfunction and degeneration. J Neurosci. 2011; 31:8306–8319. [PubMed: 21632951]

Araki T, Simon RP, Taki W, Lan JQ, Henshall DC. Characterization of neuronal death induced by focally evoked limbic seizures in the C57BL/6 mouse. J Neurosci Res. 2002; 69:614–621. [PubMed: 12210827]

Lee B, et al. The CREB/CRE transcriptional pathway: protection against oxidative stress-mediated neuronal cell death. J Neurochem. 2009; 108:1251–1265. [PubMed: 19141071]

Brandt C, Potschka H, Loscher W, Ebert U. N-methyl-D-aspartate receptor blockade after status epilepticus protects against limbic brain damage but not against epilepsy in kainate model of temporal lobe epilepsy. Neuroscience. 2003; 118:727–740. [PubMed: 12710980]

Jimenez-Mateos EM, et al. Hippocampal transcriptome after status epilepticus in mice rendered seizure damage-tolerant by epileptic preconditioning features suppressed calcium and neuronal excitability pathways. Neurobiol Dis. 2008; 32:442–453. [PubMed: 18804535]

Nagerl UV, Eberhorn N, Cambridge SB, Bonhoeffer T. Bidirectional activity-dependent morphological plasticity in hippocampal neurons. Neuron. 2004; 44:759–767. [PubMed: 15572108]

Kim CH, Lisman JE. A role of actin filament in synaptic transmission and long-term potentiation. J Neurosci. 1999; 19:4314–4324. [PubMed: 10341235]

Pavlowsky A, et al. A postsynaptic signaling pathway that may account for the cognitive defect due to IL1RAPL1 mutation. Curr Biol. 2010; 20:103–115. [PubMed: 20096586]

Wermeling DP. Intranasal delivery of antiepileptic medications for treatment of seizures. Neurotherapeutics. 2009; 6:352–358. [PubMed: 19332330]

Paxinos, G.; Franklin, KBJ. The mouse brain in stereotaxic coordinates. 2. Elsevier; San Diego, CA: 2001.

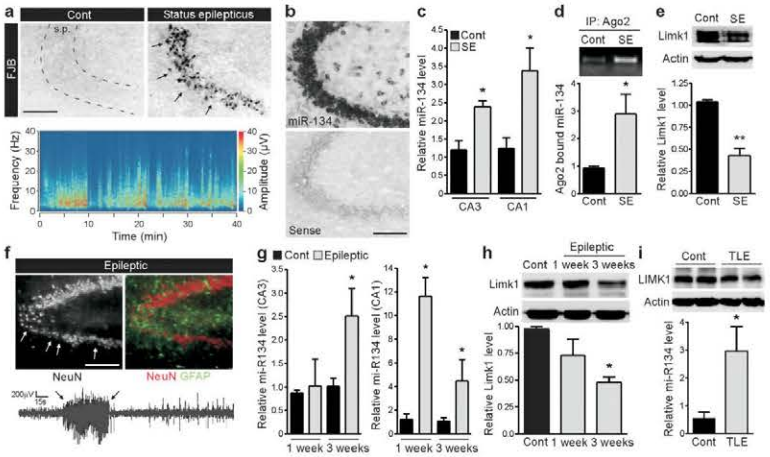

Figure 1.

miR-134 up-regulation following SE and in epilepsy. (**a**) Photomicrographs show neuronal death (Fluoro-Jade B, FJB) in CA3 stratum pyramidale (s.p.) 24 h after SE compared to control (Cont). Below, depiction of electrographic seizure frequency and amplitude during SE. (**b**) *In situ* hybridization showing miR-134 in soma of CA3 pyramidal neurons. (**c**) RT-qPCR measurement of miR-134 (normalized to RNU19) for CA3 ($P = 0.016$) and CA1 ($P = 0.035$) 24 h after SE ($n = 5$ per group). (**d**) Argonaute-2 (Ago2) –immunoprecipitated (IP) miR-134 from Cont and SE mice (24 h) ($P = 0.035$, $n = 3$ per group). (**e**) Limk1 western blot (24 h) and densitometry ($P = 0.001$, $n = 5$ per group). (**f**) Photomicrographs showing loss of CA3 neurons (NeuN, arrows) and astrogliosis (GFAP) in epileptic mice 14 days after SE and (below) a telemetry-recorded spontaneous seizure. (**g**) miR-134 levels in epileptic mice for CA3 (1 week, $P = 0.806$; 3 weeks, $P = 0.049$) and CA1 (1 week, $P = 0.003$; 3 weeks, $P = 0.008$) ($n = 5$ per group). (**h**) Western blot shows Limk1 levels 1 and 3 weeks after SE and densitometry ($P = 0.028$; $n = 4$ per group). (**i**) miR-134 levels in temporal lobe samples from individuals with TLE compared to autopsy controls (Cont) ($P = 0.029$; $n = 3$ per group). Western blot (above) shows LIMK1 levels (Unpaired *t*-test, $P = 0.039$, $n = 3$ per group, not shown). Scale bars, 200μm. $^{*}P < 0.05$, $^{**}P < 0.01$ compared to Cont.

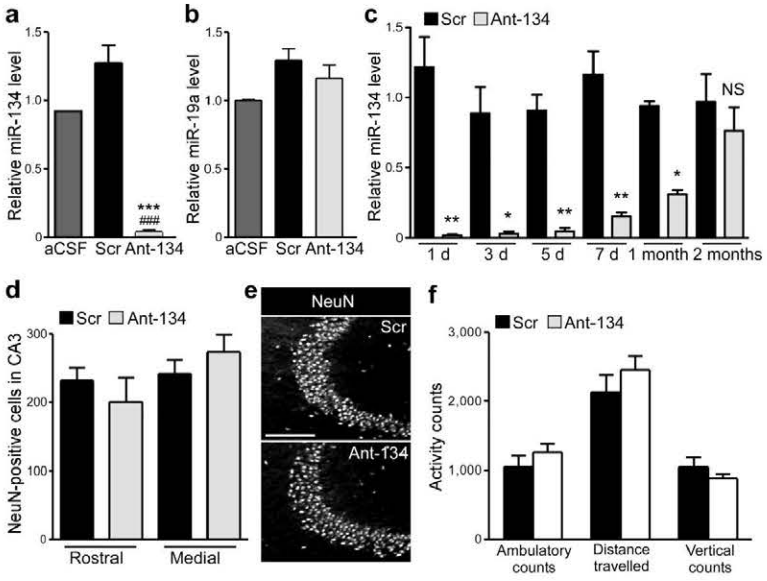

Figure 2.

Antagomir-mediated silencing of miR-134 in mouse hippocampus. (**a–b**) RT-qPCR measurement of **a**) miR-134 ($P < 0.001$) and **b**) miR-19a ($P = 0.363$) in hippocampus 24 h after i.c.v. injection of miR-134-targeting antagomir (Ant-134) or a non-targeting control (Scr). $^{***}P < 0.001$ compared to artificial cerebrospinal fluid (aCSF); $^{\#\#\#}P < 0.001$ compared to Scr ($n = 3$ per group). (**c**) miR-134 levels in hippocampus after injection of Ant-134 or Scr at 1 d ($P = 0.005$), 3 d ($P = 0.01$), 5 d ($P = 0.001$), 7 d ($P = 0.004$), 1 month ($P = 0.034$) and 2 months ($P = 0.469$) later. $^{*}P < 0.05$; $^{**}P < 0.01$; NS, non-significant ($n = 3$–4 per group). (**d**) NeuN counts at two different levels of the dorsal hippocampus in animals injected 24 h earlier with either Scr or Ant-134 (rostral, $P = 0.585$; medial, $P = 0.387$) ($n = 4$ per group). (**e**) NeuN staining of the CA3 subfield 24 h after injection of Scr or Ant-134. Scale bar: **e,** 200 μm. (**f**) Behavioral analysis of mice injected 24 h earlier either with Scr or Ant-134. Graph shows indices of exploratory activity: total ambulatory counts ($P = 0.310$); distance travelled (cm) ($P = 0.320$); vertical counts ($P = 0.300$).

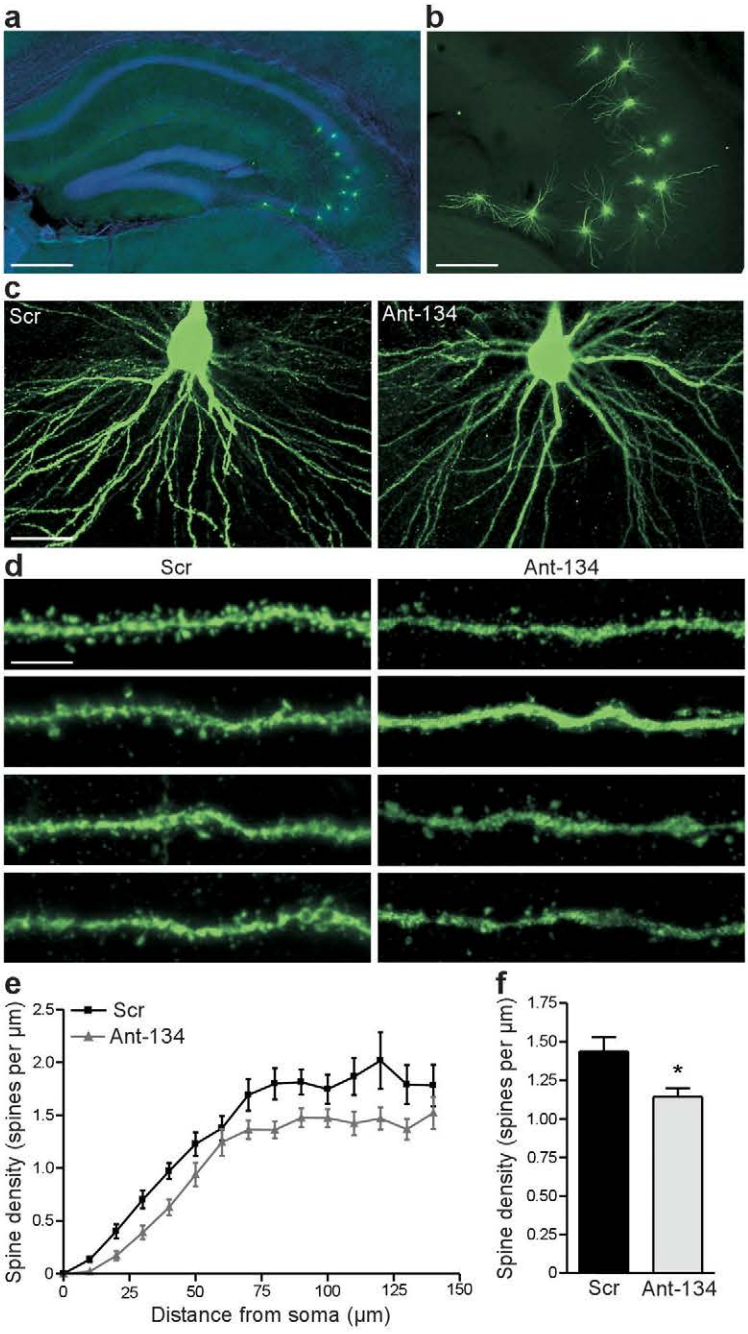

Figure 3.
Antagomir silencing of miR-134 reduces hippocampal CA3 spine density *in vivo*. (**a**) Field view of hippocampus showing Lucifer yellow-injected CA3 neurons (green) and nuclei (DAPI, blue). (**b**) Higher magnification of (**a**) showing injected CA3 neurons. (**c**) Photomicrographs of the basal tree from Lucifer yellow-injected animals treated with either Scr or Ant-134 24 h earlier. (**d**) Representative images of individual dendrites from four individual animals injected with Scr (left panels) or Ant-134 (right panels). (**e**) Spine density as a function of the distance from the soma (Sholl Analysis) for Scr and Ant-134 animals. (**f**) Spine density in Scr and Ant-134 mice ($P = 0.037$; $^*P < 0.05$ compared to Scr, $n = 7$ per group). Scale bars: **a**, 500 µm; **b**, 100 µm; **c**, 20 µm. **d**, 12 µm.

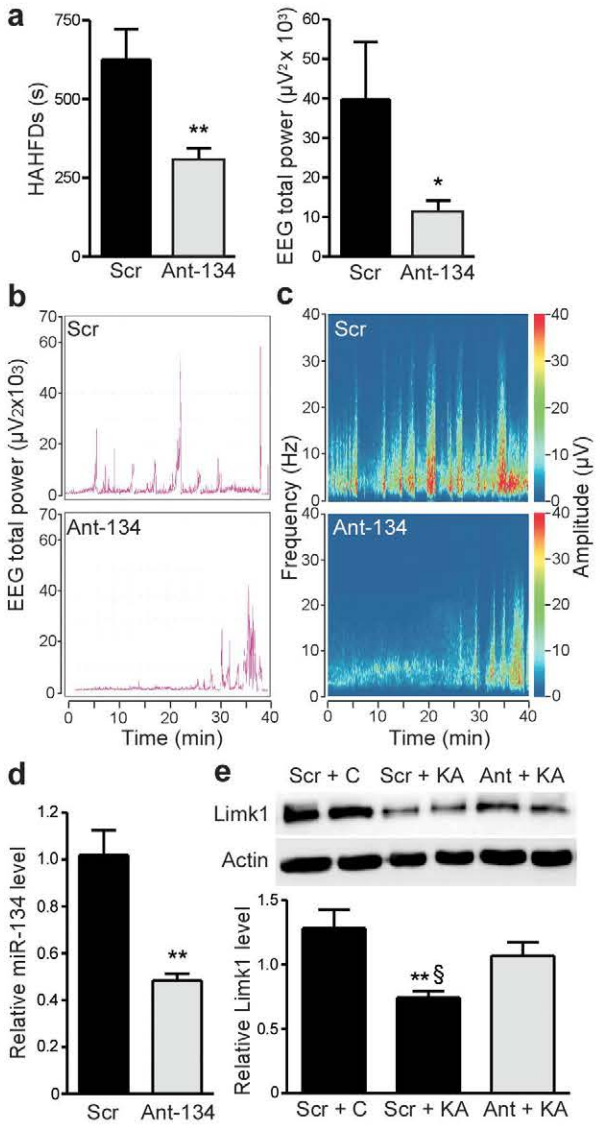

Figure 4.

Antagomir silencing of miR-134 reduces seizure severity during SE. (**a**) Graphs show HAHFDs ($P = 0.0051$) and total EEG power ($P = 0.033$) during SE in animals injected 24 h earlier with Scr or Ant-134. *$P < 0.05$, **$P < 0.01$ compared to Scr ($n = 4$–8 per group). (**b**) Total EEG power and (**c**) frequency and amplitude parameters during SE from representative Scr- and Ant-134 injected animals covering the period between KA injection and anticonvulsant administration. (**d**) miR-134 levels in Scr and Ant-134 animals 24 h after SE ($P = 0.0078$, $n = 4$). **$P < 0.01$ compared to Scr. (**e**) Limk1 protein levels in non-seizure, Scr-injected (Scr + C) and after SE in mice given Scr (Scr + SE) or Ant-134 (Ant + SE) ($n =$ 1 per lane). Graph shows Limk1 levels normalized to actin (Scr + C compared to Scr + SE, $P = 0.007$; Scr vs Ant-134 after SE ($P = 0.018$; Scr + C compared to Ant-134 + SE, $P =$ 0.270). **$P < 0.01$ compared to Scr + C; §$P < 0.05$ compared to Ant-134 + SE) ($n = 4$ per group).

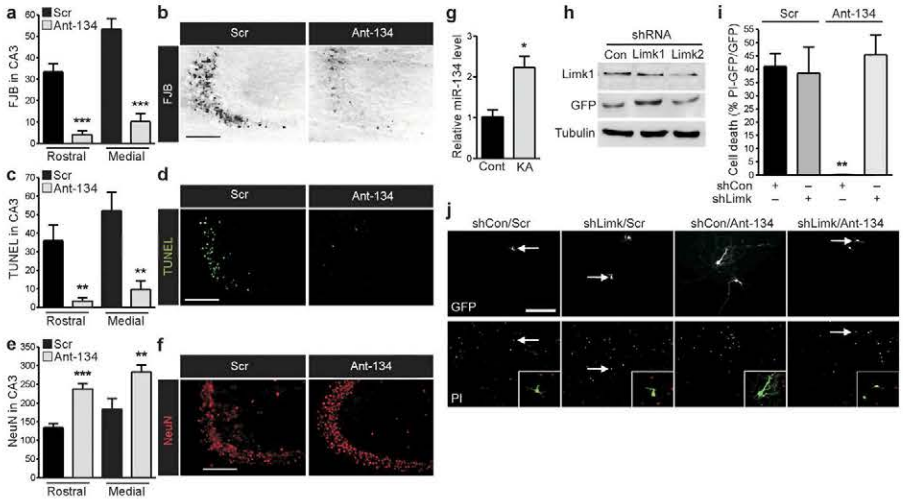

Figure 5.

Antagomir silencing of miR-134 protects against SE *in vivo* and KA toxicity *in vitro*. (**a–f**) Graphs and photomicrographs (dorsal hippocampus) 24 h after SE in mice given Scr or Ant-134 showing (**a, b**) FJB counts (rostral, $P < 0.001$; medial, $P < 0.001$), (**c, d**) TUNEL counts (rostral, $P = 0.001$; medial, $P = 0.001$), (**e, f**) NeuN counts (rostral, $P < 0.001$, medial, $P = 0.009$).$^{**}P < 0.01$, $^{***}P < 0.001$ compared to Scr ($n = 4$–8 per group). Scale bars, 200 μm. (**g**) miR-134 levels in primary hippocampal neurons 24 h after KA (0.3 μM) ($P = 0.019$). $^{*}P < 0.05$, $n = 3$ per group. (**h**) Western blots show Limk1 and GFP in SH-SY5Y cells transfected with shControl (Con) or different short interfering RNAs targeting Limk1 (shLimk1/2). shLimk2 reduced Limk1 by ~48% (average of two experiments). (**i**) Percentage cell death induced by KA in hippocampal neurons (ratio of propidium iodide (PI) positive-GFP positive neurons over GFP-positive), and effect of Scr or Ant-134 in cells co-transfected with either Con or Limk shRNA. Cell death in non-transfected neurons in either group averaged 30 ± 12% (data not shown). shCon/Scr compared to shCon/Ant-134, $P = 0.005$; shLimk/Scr compared to shCon/Ant-134, $P = 0.004$; shCon/Ant-134 compared to shLimk/Ant-134, $P = 0.001$). $^{**}P < 0.01$, $n = 4$ per group. (**j**) Photomicrographs of hippocampal neurons in each condition. Arrows (and see inset) indicate dead cells positive for both GFP (green) and PI (red). Scale bar, 50 μm.

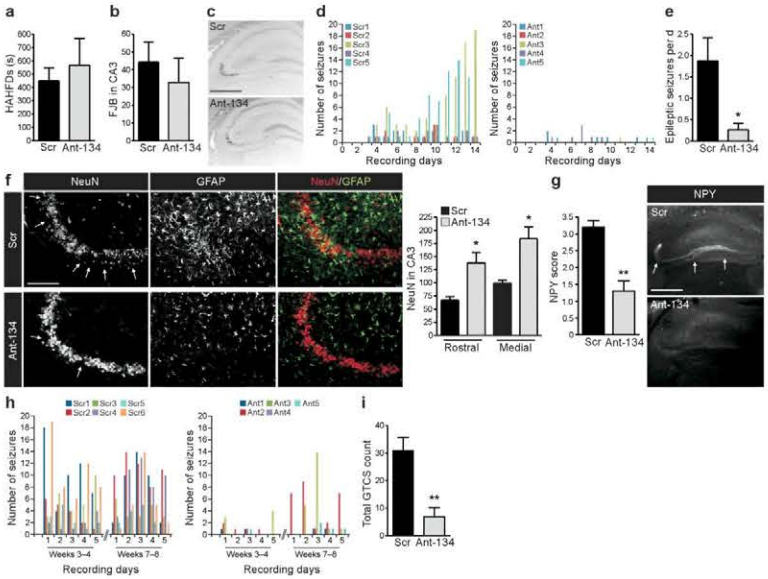

Figure 6.

Antagomir silencing of miR-134 reduces post-SE epileptic seizures and protects against progressive TLE pathology. (**a,b**) Graphs show **a**) KA-triggered seizures ($P = 0.589$) and **b**) CA3 damage at 24 h ($P = 0.541$) between Ant-134 and Scr groups when the antagomirs were injected 1 h after inducing SE ($n = 4$–5 per group). (**c**) FJB staining 24 h after SE in mice injected 1 h after KA with Scr or Ant-134. (**d**) Graphs show telemetry-detected spontaneous seizures for individual animals during the two weeks following SE for (left) Scr and (right) Ant-134 mice. (**e**) Daily epileptic seizures in Scr and Ant-134 animals ($P = 0.036$; $n = 5$ per group). (**f**) Hippocampal NeuN (arrows indicate neuron loss) and GFAP (astrogliosis) staining in Scr and Ant-134 mice after two weeks epilepsy monitoring. Graph to the right shows NeuN counts in dorsal hippocampus (rostral, $P = 0.024$, medial, $P = 0.02$) (*$P < 0.05$, $n = 5$ per group). (**g**) Neuropeptide Y (NPY) score in epileptic animals ($P = 0.008$, $n = 5$ per group) and (right) representative NPY-stained sections from Scr and Ant-134 mice after two weeks epilepsy monitoring. Scale bars: **f**, 200μm; **c, g**, 1 mm. (**h**) Graphs show the number of generalized tonic-clonic seizures (GTCS) each day for individual animals during two periods of five days continuous video monitoring following SE for (left) Scr and (right) Ant-134 mice. (**i**) Total GTCS counts averaged from the two monitoring periods (**$P = 0.003$, $n = 5$–6 per group).